UNIABUJA Journal of Engineering and Technology

https://ujet.uniabuja.edu.ng/

Special Issue

Simulation and Additive Manufacturing of a Crankshaft Component using Fused Deposition Modelling Techniques

Opeoluwa Emmanuel OWODOLU[1], Akinbode Alani OWODOLU[2], Adekunle Taofeek OYELAMI[3], Adewumi Surajudeen BABATUNDE[4], Olalekan Obadele AWOLOLA[5]

[1]Department of Mechatronics Engineering Afe Babalola University, Ekiti State, Nigeria
[2]Department of Mechatronics Engineering Federal University of Agriculture Abeokuta, Ogun State, Nigeria
[3]Department of Mechatronics Engineering Federal Polytechnic Ilaro, Ogun State, Nigeria

[1]owodoluope@abuad.edu.ng, [2]owodoluaa@funaab.edu.ng, [2]oyelamiat@funaab.edu.ng, [2]babatundesurajudeen@funaab.edu.ng, lekanoba2012@gmail.com*

Abstract
Additive Manufacturing (AM), commonly known as 3D printing, builds parts layer by layer directly from a 3D CAD model, which reduces material usage and gives designers greater flexibility than conventional methods. This study presents the design, simulation, and manufacture of an automotive crankshaft using Fused Deposition Modelling (FDM). The crankshaft ***was*** *designed in SolidWorks and exported in STL format for manufacture in PLA. The analysis* ***was*** *performed under static loading conditions to assess stress distribution, deformation, and strain, along with fatigue life. The results showed that stress concentration was highest in the fillet region and that deformation was greatest in the crankpin neck region, although both remained within the yield criteria of the material. The printed prototype showed acceptable mechanical characteristics, good dimensional accuracy, and minimal material waste. Compared with conventional subtractive manufacturing, FDM reduced cost, tooling, and lead time while still allowing the part to be customised. These findings confirm that additive manufacturing is an effective method for the rapid prototyping of automotive components and can improve industrial productivity through more sustainable manufacturing. Future work should extend the analysis to a wider range of loading conditions and materials, and validate the simulated fatigue life through physical testing before the parts are used in service.*

Keywords: Additive Manufacturing, Crankshaft, Simulation, Filament, Prototype, Modelling

1.0 Introduction

Additive Manufacturing Technique (AMT) is a production method for creating a product directly from a digital file in three dimensions that has been segmented into a series of "slices," thus allowing the additive construction of the desired product (Shahrubudin *et al.*, 2022; Singh *et al.*, 2023). This method requires only the exact amount of material necessary for the production process, thus minimising material waste compared to other subtractive production methods (Li *et al.*, 2025).

AMT is a vital production method in product development since it allows for the production of fully functional prototypes that can be used to support product concepts (Berman, 2021; Javaid & Haleem, 2022).

There are different additive production methods, but Fused Deposition Modelling (FDM) is the most commonly used additive production method due to its simplicity and cost-effectiveness. In FDM, a thermoplastic filament is unwound from a coil, heated to its melting temperature, and extruded through a nozzle onto a build platform (print bed), where it cools and solidifies layer by layer (Popescu *et al.*, 2021; González-Henríquez *et al.*, 2022). The layers already deposited form the basis for the next layers until the finished part is created.

FDM has the benefit of low start-up cost, particularly for low-level production or specialised products (Javaid & Haleem, 2022). The total cost of additive manufacturing is dependent on various factors such as build volume, material usage, and production volume (Li *et al.*, 2025). For high customisation needs, additive manufacturing is economically advantageous over traditional subtractive manufacturing methods because of lower tooling costs (Berman, 2021).

Additive manufacturing provides fewer design restrictions, high customisation, low tooling investment, and shorter time-to-market than traditional manufacturing methods (Singh *et al.*, 2023). Moreover, AM facilitates repeated production with acceptable mechanical and dimensional properties when process parameters are properly optimised (Zhang *et al.*, 2023). The applications of AM technology are wide-ranging, such as in medicine (personalis ed implants and prosthetics), aerospace parts, food printing, arts, and car manufacturing (Shahrubudin *et al.*, 2022). In the car industry, the incorporation of 3D printing has enhanced

Received: 27-05-2026 / Accepted: 11-06-2026 / Published: 20-07-2026

https://doi.org/10.70118/ujet.2026.sp01.09

the product development process through quick prototyping, frequent function testing, and quick design iteration (Berman, 2021; Kumar *et al*., 2024).

This research involves designing a crankshaft in the form of a 3D model using a computer-aided design tool called SolidWorks and saving it in STL format for printing. An additive manufacturing process is employed to create a crankshaft model using a PLA (Poly Lactic Acid) material in an FDM 3D printing process. In this process, the material is laid down layer by layer to create a crankshaft model. This process is used due to the biodegradable nature of the material, which is suitable for FDM technology (González-Henríquez *et al*., 2022).

Additive manufacturing is used to overcome issues faced by subtractive manufacturing technology, such as excessive material wastage and the high cost of production (Popescu *et al*., 2021).

The aim of the study is to quickly manufacture an efficient crankshaft prototype designed using FDM, with minimal material waste. Conventional crankshafts are manufactured using time-consuming and expensive processes due to material removal operations and tooling requirements (Kumar *et al*., 2024). The objectives of the study are to design and simulate the crankshaft model, export the model in STL format, and manufacture it using PLA material via FDM.

The significance of the study lies in the reduction of lead time, enhanced availability of simple and complex parts, high degree of customization, and reduced production costs due to minimal material waste and flexibility in the manufacturing process (Javaid & Haleem, 2022; Li *et al*., 2025). Finally, the significance of the study lies in the overall efficiency, competitiveness, and development of the economy. Additive manufacturing, also known as '3D Printing', has experienced tremendous evolution in the last decade, quickly becoming a revolutionary manufacturing process in various industries. AM techniques are employed to manufacture products layer by layer using digital 3D models, resulting in minimal material waste and the ability to produce complex geometries, which are difficult to manufacture using conventional subtractive manufacturing processes (Ngo et al., 2021). In particular, AM technologies like FDM have been prominent due to their accessibility and adaptability to various thermoplastic materials.

According to Shahrubudin *et al*. (2022), the current AM process consists of the following steps: (1) CAD modelling; (2) slicing; (3) material deposition; and (4) post-processing. The slicing method provides greater freedom and customizability with faster production times for prototype and small-batch manufacturing (Yeshiwas, 2025).

FDM has been one of the most commonly used AM technologies due to its simplicity and cost-effectiveness. FDM technology involves the extrusion of thermoplastic materials through a heated nozzle and deposition of the material on a build platform to produce the desired shape (Popescu *et al*., 2021). The recent trend of research has been on the comprehension and enhancement of FDM technology.

Sapkota *et al*. (2024) reviewed FDM process conditions. They studied the importance of material properties, temperature conditions, and process parameters like layer thickness, temperature of the nozzle, and printing speed in improving the mechanical properties of FDM parts.

Another research article by Zeng *et al*. (2025) discussed the research progress in FDM technology worldwide. They discussed the recent research trends in the development of FDM materials, hybrid FDM techniques, and the use of intelligent control systems in FDM. They discussed the importance of using real-time monitoring systems in FDM.

Equbal *et al*. (2024) discussed the dimensional accuracy of FDM parts. They discussed the importance of minimizing warpage, layer adhesion defects, and temperature distortions in FDM parts. They mentioned that these defects can be minimized using the best equipment available in the market as well as the environmental conditions. With smart algorithms, print quality can be significantly enhanced.

The choice of material is an essential factor in determining AM process performance. PLA (polylactic acid), ABS (acrylonitrile butadiene styrene), and other thermoplastics are widely studied in FDM due to their extrudability and thermal properties (González-Henríquez *et al*., 2022). Recent research is now opening up material properties by developing and utilising composites and specific compound materials for enhanced functional properties

Galib *et al*. (2025) have extensively studied and reviewed various composite materials and their uses in AM processes, including FDM. The benefits of utilising composite materials in FDM are that they have better mechanical properties due to reinforcement of fillers and better printability. The research shows that composite materials are becoming more popular in various industries, such as automotive, aerospace, and tooling industries, where high-strength and lightweight are required.

El-Zathry *et al*. (2026) have studied and reviewed various machine learning methods for quality improvement in AM processes. The researchers have shown that various predictive model techniques, such as Artificial Neural Networks (ANN), can be applied for better correlation of process variables and final part properties.

Recent research has also gone beyond the basics of process descriptions to include advanced optimisation techniques. Rashid & Koç (2021) investigated the numerical simulation methods for Fused Filament Fabrication (FFM). Simulation methods can assist in the prediction of temperature distribution and material flow, as well as the deformation of the parts to be created before the actual printing process. This can assist in the reduction of trial and error in the process as well as the optimisation of the materials used.

Tudorache *et al*. (2025) discussed the digital twin concepts in the process of additive manufacturing. The use of digital twins in the process shows the shift in the process toward the use of Industry 4.0. Omer (2025) discussed the recent advances in the process of interlayer bonding in FDM. Interlayer adhesions play a critical role in the overall strength of the parts created in the process.

The versatility of AM in rapid prototyping has a significant impact on various industries. For example, in the medical field, AM is used for patient-specific implants, anatomical models for surgery planning, and prosthetics (Ali *et al*., 2024). For the automotive industry and the aerospace industry, AM is used for lightweight structural parts, tooling parts, and functional prototypes with reduced time to market (Berman, 2021). Yeshiwas (2025) also points out the interdisciplinary applications of AM. For example, AM is used in food printing, the arts, architectural modelling, and even in consumer electronics. The versatility of AM is due to the maturity of the technology as well as the confidence in the accuracy and reliability of the AM process. Despite the advantages offered by AM and FDM in particular, there are still some hurdles to overcome. For example, the behavior of the materials used in AM is still an area for further research. Singh *et a*l. (2023) highlight the variability in the behaviour of materials used in AM and suggest that the development of advanced materials with real-time monitoring is the way forward.

2.0 Materials and Methods

The design, material, and method and process of making the crankshaft prototype are discussed in this paper.In this design, some of the parts of the crankshaft include the following: crank pin, crank web, and shaft. The three forces acting on the crankshaft cause bending and torsion moments include the connecting rod force acting on the crank pin, the weight of the flywheel acting vertically downward, and the belt tensions acting horizontally. Plain carbon steels and alloy steels are the materials most often used for making the crankshafts. The 40C8 is a simple carbon steel material. As this is a new design method, the prototype was produced using PLA filament. Quality materials have to be used for making quality gadgets using the 3D printing method. The usage of multiple materials along with the 3D printing method helps in making quality products. For this paper, the model of the crankshaft is designed using Solid-Works software and saved in STL format. In this paper, the fused deposition modelling AM technique is used. The finalised SolidWorks model has a bounding box of 50 mm (X-axis) × 67.5 mm (Y-axis) × 317 mm (Z-axis, along the crankshaft axis of rotation), with a computed volume of 2.3391×10^{-4} m^3. The model was exported in STL format for import into ANSYS via the SpaceClaim interface and separately into the slicing software for FDM fabrication.

1. Filament

The filament used in the three-dimensional printing process has a diameter of either 1.75 mm or 3 mm. The material used in the printing process is in the form of wire. The motor is used to feed the filament to the extruder. There are many different sizes available in the materials used in the filament. Some materials are made up of plastic materials such as polyamide (PA), acrylonitrile, butadiene styrene (ABS), polystyrene (PS), polycarbonate (PC), and poly-lactic acid (PLA). The quality of the product depends upon the type of material used in the printing process. The quality is further influenced by the resistance to heat, chemical, and mechanical elements. The filament used is available in different colours.

A. Properties of Poly Lactic Acid [PLA]

The PLA products are more eco-friendly. The biocompatibility of PLA with the human body is one of its other excellent properties. The PLA has a tougher structure than ABS and melts at a lower temperature than ABS, between 180 and 220°C. It was chosen for this project because its glass transition temperature ranges from 60 to 65°C. The properties of PLA used are shown in Table 1

https://doi.org/10.70118/ujet.2026.sp01.09

Table 1. Comparative material properties: Structural Steel (ANSYS simulation) versus PLA (FDM prototype fabrication).

Property	Unit	Structural Steel (ANSYS Simulation)	PLA (FDM Prototype)
Density	kg/m³	7,850	1,300
Tensile Yield Strength	MPa	250	50
Tensile Ultimate Strength	MPa	460	50–60
Young's Modulus	GPa	200	2.0–2.6
Poisson's Ratio	N/A	0.30	~0.36
Shear Modulus	GPa	76.92	2.4
Coeff. Thermal Expansion	$°C^{-1}$	1.2×10^{-5}	$\sim 6.8 \times 10^{-5}$
Thermal Conductivity	W/m·K	60.5	0.13
Specific Heat	J/kg·°C	434	1,800
Role in This Study	N/A	FEA only	FDM fabrication only

2. The 3D Printer

The 3D printer used is shown in Figure1. It has different parts coupled together.

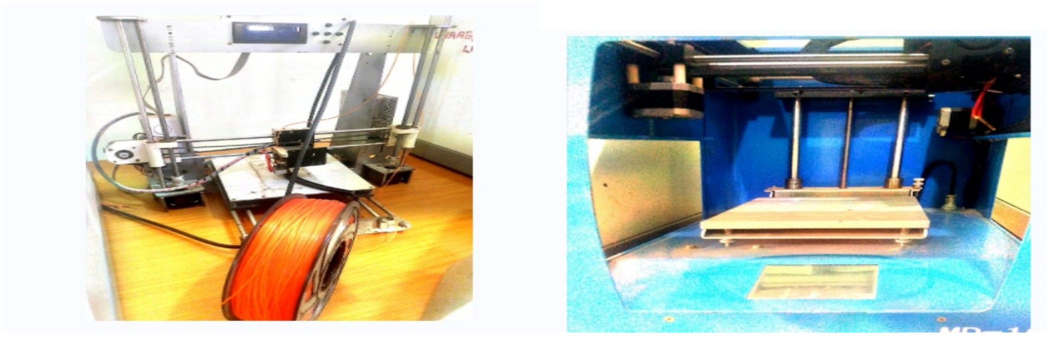

Figure 1: 3D Printers

There is a level area on the print bed. The fused filament is deposited there by the extruder in solid form. Depending on the filament or substance used, the bed is heated during printing. Most of the print beds are made up of aluminium material. Moreover, it is also easy to get a glass print bed.

B. Extruder

The part that supplies heated filaments to the bed is called the extruder. It is very significant in this printing process, as the filament first melts in the extruder. As a result of heating, the filament melts and sticks to the print bed. The nozzle, or extruder tip, is a very essential part of the extruder. The melted filament sticks appear through the nozzle on the print. The nozzle size varies from 0.25 mm to 0.75 mm. The most commonly used nozzle size is 0.5 mm. This is demonstrated in Figure 1.

C. Motherboard or controller

The mother board or controller regulates the 3D printer process. It controls the motion or action that the 3D printer's parts display. Processing G-code commands. the Z-axis motors are essentially connected to the same stepper motor controller, which regulates and controls the four stepper motor controllers. By observing the end-stops, the temperature of the heated bed is controlled. A USB-to-serial converter is used to link the electronics board to the PC in Figure 1.

D. Some other components of a 3D Printer

Other than the above-mentioned components, the 3D printer has some other functional parts, which include stepper motors, Y-axis stepper motor controllers, bushings for the X-carriage extruder, end stops, Z-axis and Y-axis print plate, electronics components, and frame (Figure 1).

E. The Frame

The frame holds other components and supports the printer. The printer's three axes are added to the frame. Threaded rods and printed parts are assembled to form the frame. Along with the vertices, the edge also includes printed components that hold and replicate the Y-axis and Z-axis. The stepper motors for the Z-axis are held by the printed parts in the upper left and upper right corners.

The Y-axis is only able to move in one direction, or between the front and back of the case. A belt drive attached to a stepper motor with a pulley controls the Y-axis. Four bushings are connected to the print base

https://doi.org/10.70118/ujet.2026.sp01.09

plate. The only type of bearings are bushings. They pass across the slick bars. The bearing includes tiny balls inside and only allows for free.

F Stepper Motor

The 3D printer has five stepper motors. One motor is for the Y axis, one is for the extruder, and two are for the Z axis, and finally, one is for the X axis.

G. Stepper Motor Controller

It is difficult to control a bipolar stepper motor, especially when working on a small scale. Unipolar stepper motors are easier to control, but even though they are of the same size, they are unable to provide a greater amount of torque. The difficulties in controlling a stepper motor are removed by making use of exceptionally designed stepper motor controllers. With the use of this controller, some moderate steps are taken.

3. Operation of 3D Printer

After that, the files are converted into the STL format and the STL file is sliced as it is loaded into the printer according to specifications, Once the material which is the filament is available. the filament begins to melt within the extruder as it begins to heat up. The prototype of the crankshaft is built layer on top of the other on the print bed as the filament melts. The formation of layer by layer continues until the finished product of crankshaft is made then the process ends. as shown in Figure2.

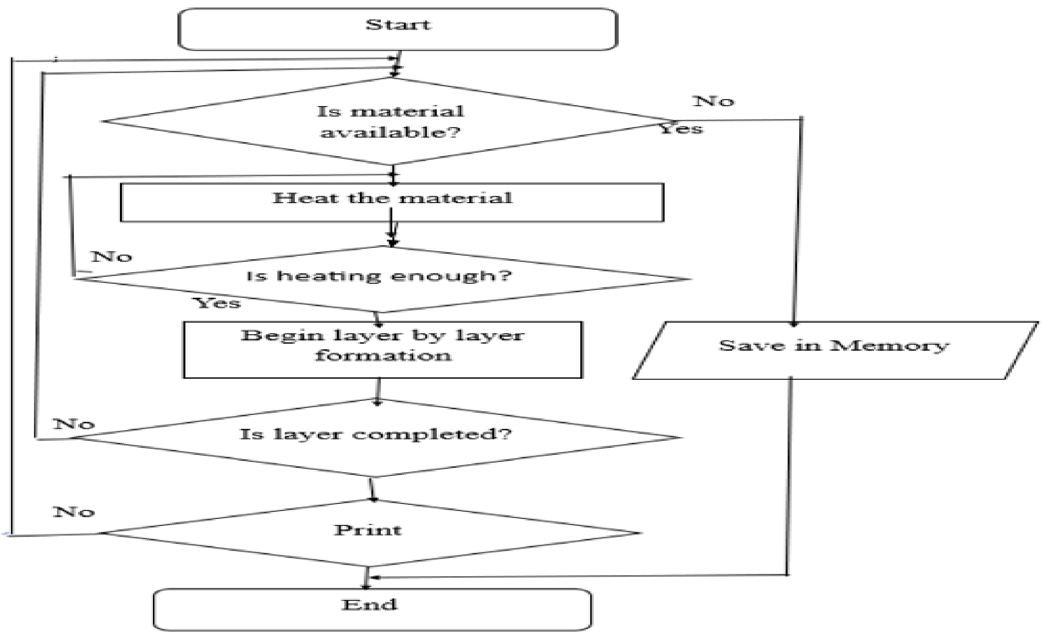

Figure 2: Additive Manufacturing Flow Chart of Crankshaft.

As a result, the way a stepper motor is controlled has changed. END STOPS: All three axes need to be moved from the beginning position to the starting position before the object is printed and back when the printing process ends in the program

4.. Stages of Production of Crankshaft Prototype

i The Design Stage: This is the first stage. At this stage, the SOLIDWORKS software program is being used to design the crankshaft in three dimensions3D on a computer system.

ii. Transformation Stage: The 3D drawing is transformed into stereolithography (STL) format in the second stage: This is accepted practice.

iii. STL files slicing Stage: At this stage, a pre-processing computer application that reads the STL format is used. Depending on the construction technique, the pre-processing program divides the stereolithography model into several layers ranging in thickness from 0.01 mm to 0.7 mm. The application also creates a support framework to assist the 0.02 model while it is being built. Complex structures inevitably need supplemental support.

iv. Construction of Real crankshaft prototypes: This involves the construction of crankshaft prototypes in layers stage with the filament employing fused deposition additive manufacturing processes as shown in Figure3.

.

https://doi.org/10.70118/ujet.2026.sp01.09

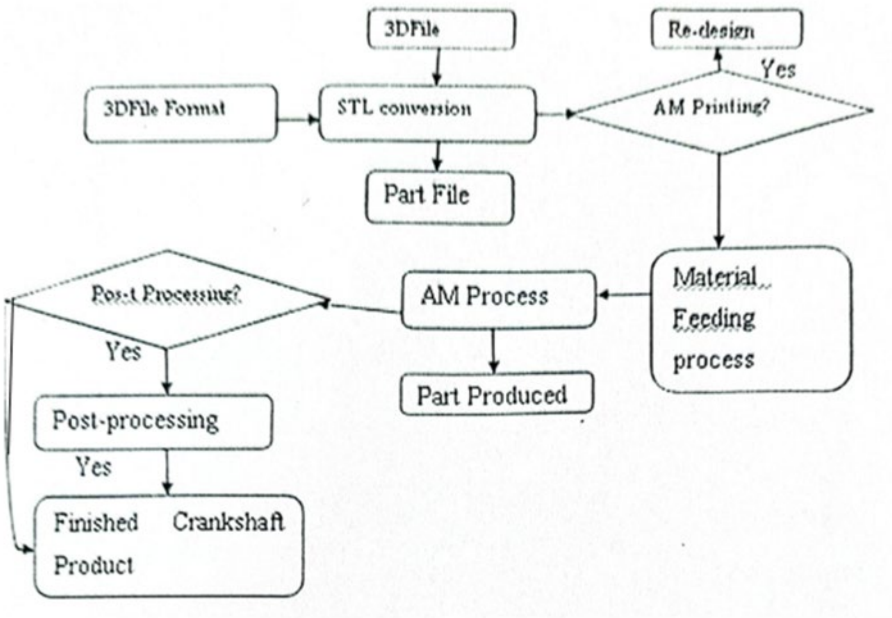

Figure 3: *Shows the Flowchart of the Additive Manufacturing Technique*

5. Printing

Firstly, a slicer slices a 3D model into small layers and produces a G-code file from a STL file that contains instructions for a printer. A model is developed through a series of cross-sections by a 3D printer through a process of following G-code instructions to deposit layers of liquid, powder, or sheet material. The ultimate shape of a model is produced through a union or fusion process of layers produced by a 3D printer. This process is called 'fused deposition modelling'.

6. Fused Deposition Modelling (FDM) Principle

The AM in this work used the fused deposition modelling. In this process, layers of a crankshaft model are produced through the deposition of filament material that hardens. For this process, a coil of wire or plastic filament is unwound to provide material to an extrusion nozzle head, as shown in Figure 4.

The material used in the filament is heated to a specific temperature using the nozzle head. The head also regulates the flow. The head is usually moved in the z-direction using stepper motors. The motors are used to regulate the flow to the specified requirements. A program in a microprocessor/microcontroller regulates the mechanism. The head can be moved both horizontally and vertically, as shown in Figure 4.

https://doi.org/10.70118/ujet.2026.sp01.09

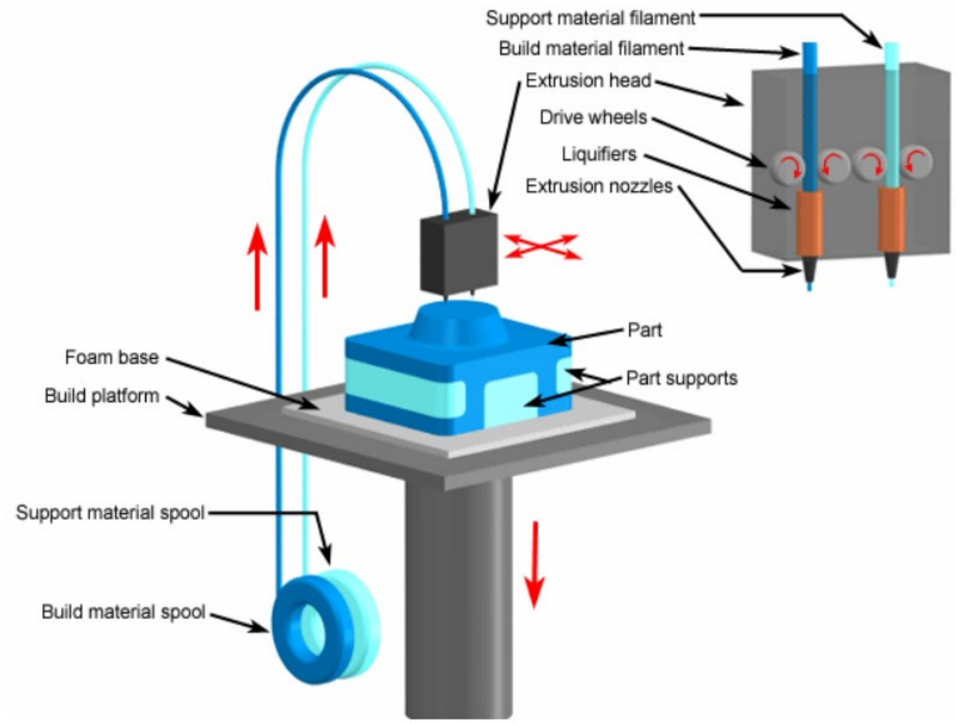

Figure 4: Filament Extrusion

A. Modelling

With the help of the computer program "SolidWorks," the 3D model is created. The modelling procedure used the data to provide geometry for 3D computer graphics. Analysing and gathering information about the object's shape and appearance is the process of 3D modeling and is saved in STL format, the 3D model as in Figure 5.

B. Selection of Technique

Fused Deposition Modelled additive manufacturing was selected for the project as it was the most simple, accessible, and cost-effective currently. The AM technology provides numerous opportunities for both professional and non-professional applications. It benefits from low-cost raw materials and a wide variety of thermoplastics, and is used for all types of modelling purposes.

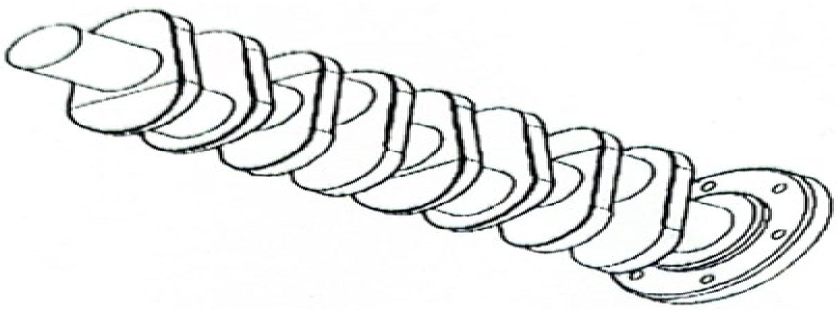

Figure 5: Modelled Crankshaft with Fused Deposition

Table 2. shows how bed adhesion was enhanced by applying two layers of polyvinyl alcohol (PVA) glue stick to the build surface prior to each print, a practice found to reliably prevent first-layer detachment in large, geometrically asymmetric parts such as the crankshaft.

https://doi.org/10.70118/ujet.2026.sp01.09

Table 2: PLA filament properties and FDM printing parameters used for crankshaft prototype fabrication.

Parameter / Property	Value	Unit
Filament diameter	1.75	mm
Nozzle temperature	180	°C
Bed temperature	60	°C
Layer height	0.2	mm
Print speed	50	mm/s
Infill density	40	%
Bed adhesion method	PVA glue stick (×2 layers)	N/A
Density	1,300	kg/m³
Tensile Yield Strength	50	MPa
Young's Modulus	2.0–2.6	GPa
Flexural Strength	80	MPa
Flexural Modulus	4.0	GPa
Glass Transition Temperature	60	°C
Melting Point	160	°C
Thermal Conductivity	0.13	W/m·K
Specific Heat Capacity	1,800	J/kg·K

7. ANSYS FEA Simulation Configuration

Static structural analysis was conducted in ANSYS Workbench 2023 R1 using the MAPDL solver in the metric (mks) unit system. The crankshaft geometry, imported via the SpaceClaim interface from the SolidWorks STL export, was assigned structural steel material properties as described in Section 3.2. Meshing was performed using automatic adaptive sizing at a resolution of 2, with a body sizing control applied at an element size of 4 mm. The resulting mesh comprised 53,863 nodes and 33,099 elements, and mesh quality was verified against ANSYS aggressive mechanical error limits to ensure solution fidelity. The environment temperature was set to 22°C to reflect ambient laboratory conditions. A single-step static analysis was configured with an end time of 1.0 s and program-controlled auto time-stepping.

The boundary conditions applied to the model, summarised in Table 3, were selected to represent a simplified but physically meaningful prototype loading scenario. Fixed supports were applied to the two main journal face sets, constraining all six degrees of freedom at those surfaces, consistent with the physical constraint imposed by engine block bearing supports. A ramped pressure load of 2.3452×10^5 Pa, applied normal to seven crankpin surface faces via a surface-effect formulation on the deformed area, represented a representative gas-pressure-derived force acting on the crankpin. For the fatigue analysis, a fully reversed constant amplitude loading ratio of $R = -1$ was adopted, representing the worst-case scenario of equal tensile and compressive stress amplitude, a conservative and standard assumption for rotating machinery components (Rashid & Koç, 2021). The Gerber parabolic mean stress correction theory was applied, and the design life was specified as 1×10^9 cycles. Structural steel S-N curve data from the ANSYS material library were used directly

https://doi.org/10.70118/ujet.2026.sp01.09

Table 3: ANSYS 2023 R1 simulation boundary conditions and analysis settings.

Boundary Condition	Type	Scope	Value / Setting
Fixed Support	Displacement constraint	2 main journal face sets	All DOF = 0
Pressure Load	Force (pressure)	7 crankpin surface faces	2.3452×10^5 Pa (ramped)
Load direction	N/A	Normal to surface	Surface effect, deformed area
Analysis steps	N/A	1 step	End time = 1.0 s
Environment temperature	Thermal	Global	22°C
Mesh element size	Body sizing	Full body	4 mm
Mesh nodes and elements	N/A	N/A	53,863 / 33,099
Fatigue loading type	Constant amplitude	Global	Ratio R = −1 (fully reversed)
Fatigue mean stress theory	N/A	N/A	Gerber parabolic
Fatigue stress component	N/A	N/A	Equivalent (von Mises)
Design life	N/A	N/A	1×10^9 cycles
Life units	N/A	N/A	1 unit = 1×10^6 cycles

8. Stress and Deformation of Solid

Unlike the stresses in fluids, the stresses in solid gradient functions of deformation, like the velocity rates of deformation. The stresses in a solid are in a fixed grid, like the stresses in a fluid; thus, the reference is to the Eulerian deformation gradients. It is important to refer to this configuration, which is defined by the fact that X=XI, X2, X3..., which are the material location points at the period or time of filament solidification. For material location point change with the velocity, u is the displacement vector, the new configuration for reference Xj and current configuration (x) and F maps infinitesimal line elements are expressed by the following equations:

$$dx = F.dX \qquad \text{...Equation 1}$$

$$F= \frac{\partial x}{\partial X} = 1 + \nabla x^{u} \qquad \text{...Equation2}$$

AM technique makes designed product possible based on scaled or actual size, depending on the application. The advantages at this stage are the elimination of the limitations of other technologies, shorter manufacture time, a rationalisation of the cost and a lower cost of design changes.

3.0 Results and Discussion

The results of this study are organised into four subsections. Sections 4A and B present and discuss the static structural and fatigue simulation outputs from ANSYS, with each result interpreted in its engineering context. Section 4C addresses the material discrepancy between the simulation and the physical prototype, providing a transparent quantitative justification. Section 4D assesses the physical FDM prototype and presents a comparative evaluation of FDM against conventional manufacturing. Throughout, results are cross-referenced with the existing literature to situate the findings within the broader field.

A. *Static Structural Analysis*

The static structural analysis includes total deformation, directional deformation, equivalent elastic strain, and Von Mises stress, which together characterise the complete mechanical response of the crankshaft to the applied pressure load as shown in Table 4.

https://doi.org/10.70118/ujet.2026.sp01.09

Table 4: Static structural analysis results. Material: Structural Steel. Applied pressure: 2.3452×10^5 Pa on 7 crankpin faces.

Output Parameter	Minimum	Maximum	Average	Unit
Total Deformation	0.000	4.6285×10^{-8}	1.5914×10^{-8}	m
Directional Deformation (X-axis)	-8.3552×10^{-9}	8.2719×10^{-9}	-3.212×10^{-11}	m
Equivalent Elastic Strain	2.7009×10^{-10}	1.349×10^{-6}	3.013×10^{-7}	m/m
Equivalent (Von Mises) Stress	29.651	2.6979×10^5	57,356	Pa

B. Total Deformation

The total deformation field, illustrated in Figure 6, reveals a maximum displacement of 4.6285×10^{-8} m (approximately 46.3 nm) occurring at the midpoint of the crankpin, the geometric centroid of the loaded surface and the location furthest from the boundary conditions constraining motion at the main journals. The minimum deformation of zero, as expected, occurs at the fixed support faces. The average deformation. . across the entire body is 1.5914×10^{-8} m. To place this result in physical context: the maximum displacement of 46.3 nm represents approximately 0.0001% of the crankshaft's axial length of 317 mm. This extraordinarily small deformation magnitude reflects the high stiffness of the structural steel model relative to the applied prototype load, a finding entirely consistent with the vast disparity between the applied pressure (0.23 MPa) and the material's Young's modulus (200 GPa).

The deformation contour follows the expected pattern for a shaft under eccentric loading: maximum at the unsupported crankpin midpoint, diminishing toward the journal bearing seats, with a smooth gradient along the crank web. This pattern is consistent with classical elasticity solutions for eccentrically loaded shaft segments (Kumar et al., 2024).

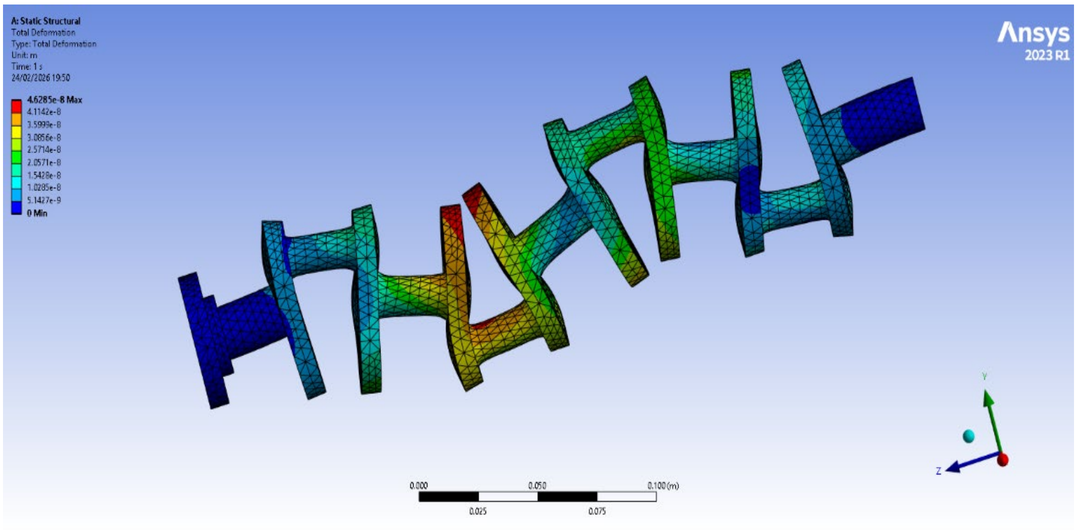

Figure 6: Total deformation contour of crankshaft under applied crankpin pressure.

C. Directional Deformation (X-Axis)

The X-axis directional deformation ranges from -8.3552×10^{-9} m to $+8.2719 \times 10^{-9}$ m, with an average of -3.212×10^{-11} m, a value so close to zero as to be numerically negligible. The near-perfect antisymmetric of the directional deformation about the crankshaft's axial plane is a valuable validation indicator: it confirms that the model's boundary conditions impose no net lateral force or moment and that the mesh and material assignment are geometrically consistent. Any significant departure from this antisymmetric would suggest a modelling error in the support application or geometric asymmetry in the mesh, neither of which is observed

https://doi.org/10.70118/ujet.2026.sp01.09

here. The magnitudes involved (sub-nanometre lateral displacements) further confirm that lateral bending under the applied prototype load is negligible as shown in Figure7.

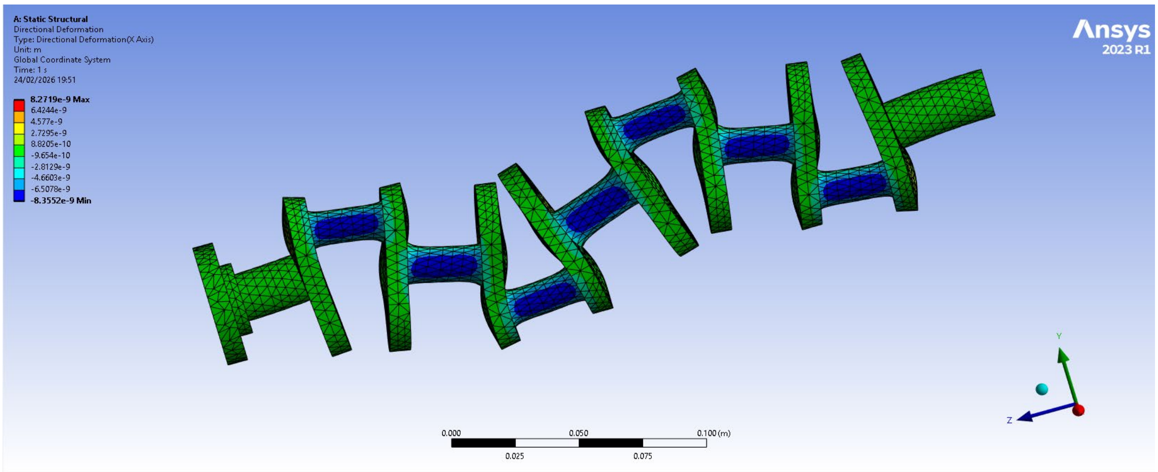

Figure 7: X-axis directional deformation. Range: -8.3552×10^{-9} m to $+8.2719 \times 10^{-9}$ m.

D. *Equivalent Elastic Strain*

The equivalent elastic strain distribution, shown in Figure 8, spans nearly four orders of magnitude across the crankshaft body: from a minimum of 2.7009×10^{-10} m/m at the crank web extremities and shaft ends to a maximum of 1.349×10^{-6} m/m at the crankpin midpoint. The average strain of 3.013×10^{-7} m/m reflects the moderate overall loading of the component. The strain concentration at the crankpin is physically expected: this surface receives the applied pressure load directly, and the eccentric geometry of the crankpin relative to the main journal axis produces a bending moment whose magnitude peaks at the crankpin midspan, driving the highest fibre strains at that location. The crank web, which connects the crankpin to the main journal, shows intermediate strain values consistent with its role as a load-transferring shear element. Critically, the maximum strain of 1.349×10^{-6} m/m is more than three orders of magnitude below the elastic strain limit of structural steel (yield strain in Equation 3 which confirms that the entire crankshaft body operates within the linear elastic regime and that no plastic deformation is predicted at any location.

$$\epsilon_y = \frac{\sigma_y}{E} = \frac{250 \ x \ 10^6}{200 \ x \ 10^9} = 1.25 \times 10^{-3} \ m/m) \qquad \text{... Equation 3}$$

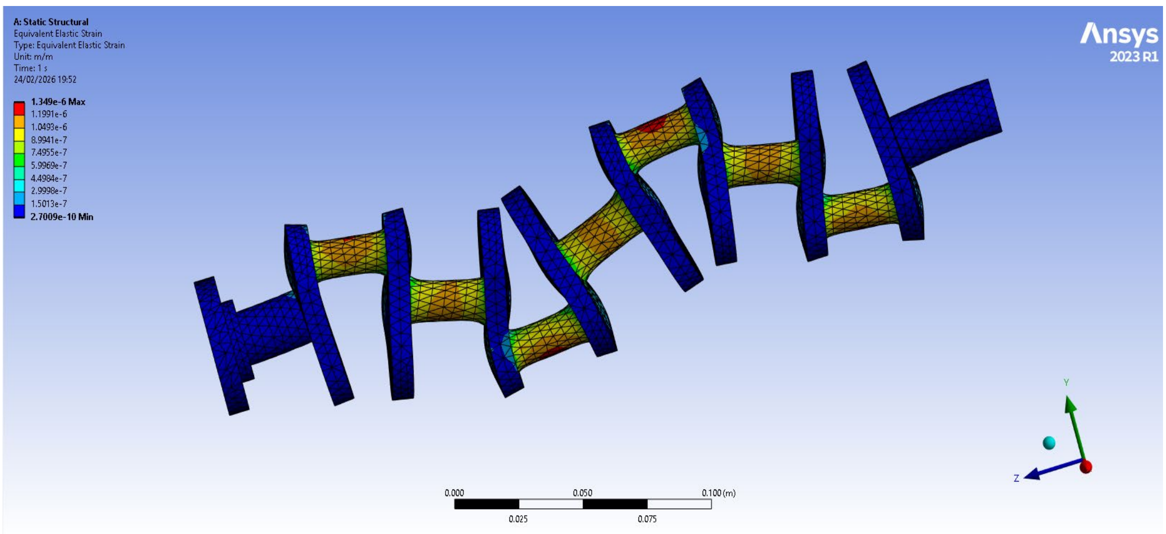

Figure 8: Equivalent elastic strain distribution.

https://doi.org/10.70118/ujet.2026.sp01.09

E. Equivalent (Von Mises) Stress

The Von Mises stress distribution, depicted in Figure 9, reveals a maximum equivalent stress of 2.6979×10^5 Pa (0.270 MPa) concentrated at the fillet transition between the crankpin journal and the crank web, a location universally recognised as the primary stress concentration zone in crankshaft design, arising from the geometric discontinuity at the change in cross-section (Kumar *et al.*, 2024). The main journal edges also exhibit locally elevated stress, reflecting the constraint-induced stress concentration at the fixed support boundaries. The body-average stress of 57,356 Pa (0.057 MPa) demonstrates that the bulk of the crankshaft volume is only lightly stressed, with the elevated values confined to narrow zones at geometric transitions.

The safety margin against yield failure is remarkable: the maximum Von Mises stress of 0.270 MPa represents only 0.108% of the structural steel yield strength of 250 MPa, representing a factor of safety against yielding exceeding 925. This extreme margin is a direct consequence of the prototype-scale applied load (0.235 MPa pressure), which is substantially lower than the combustion pressures of approximately 5–10 MPa encountered in operational automotive engines. The simulation therefore confirms that the crankshaft geometry, when fabricated in structural steel and subjected to the applied prototype load, exhibits a fully elastic, structurally safe response with no risk of yielding or permanent deformation. These results also establish that the geometry itself is not a structural weakness under the conditions tested, and that any failure mode at higher loads would be governed by the fillet stress concentration rather than by bulk section insufficiency, a finding consistent with the known failure mechanisms of operational crankshafts (Kumar *et al.*, 2024).

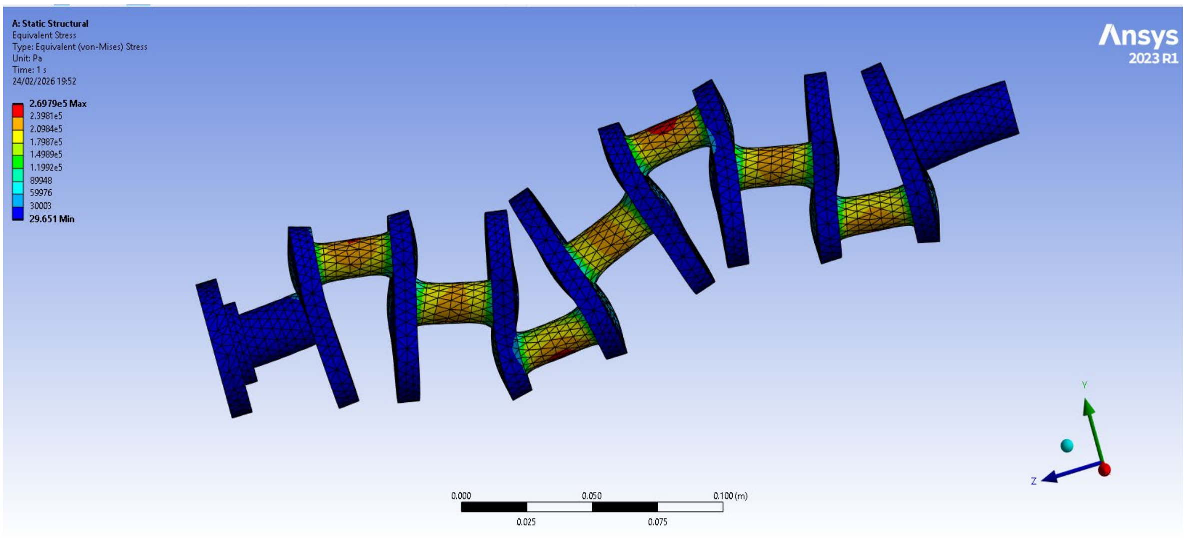

Figure 9: Equivalent Von Mises stress distribution. Maximum = 2.6979×10^5 Pa (0.270 MPa) at the fillet between the crankpin journal and the crank web (red).

F. Fatigue Analysis

Fatigue failure, defined as the progressive damage accumulation and eventual fracture of a material under repeated cyclic loading, is the dominant failure mode of rotating machinery components, including crankshafts. The ANSYS fatigue tool was employed to evaluate the crankshaft's resistance to fatigue under the applied loading cycle, using the S-N (stress-life) approach, Gerber mean stress correction, and a fully reversed load ratio of R = −1. The complete fatigue results are presented in Table 5.

https://doi.org/10.70118/ujet.2026.sp01.09

Table 5: ANSYS fatigue analysis results

Fatigue Output Parameter	**Minimum**	**Maximum**	**Average**	**Unit**
Fatigue Life	1×10^{12}	1×10^{12}	1×10^{12}	cycles
Fatigue Damage Index	1×10^{-3}	1×10^{-3}	1×10^{-3}	dimensionless
Safety Factor	15	15	15	dimensionless
Biaxiality Indication	−0.99996	0.99986	7.508×10^{-2}	N/A
Equivalent Alternating Stress	29.651	2.6979×10^5	57,356	Pa

Method: S-N Stress Life, Gerber mean stress correction, R = −1 (fully reversed), Design Life = 1×10^9 cycles, Kf = 1.0. Stress component: Equivalent (Von Mises).

G. Fatigue Life and Damage

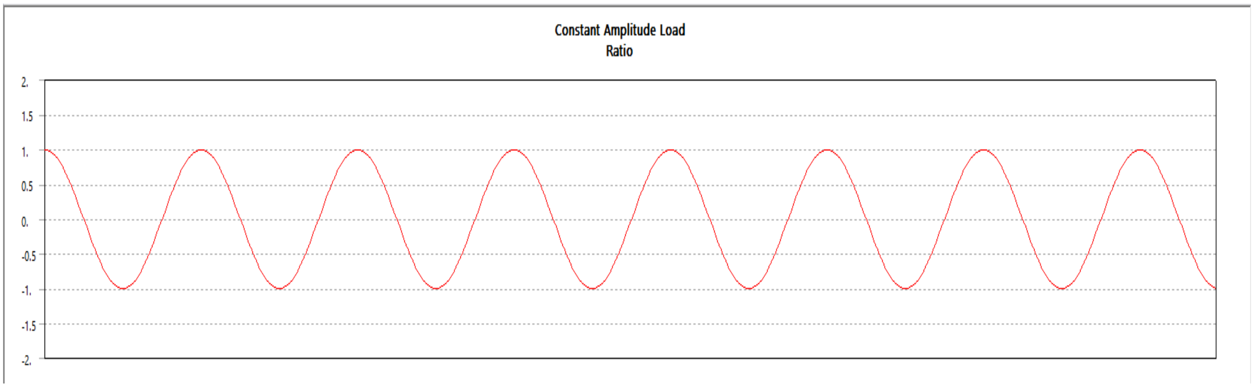

Figure 10: Fatigue life distribution. Uniform value of 1×10^{12} cycles across entire body

Figure 11. Shows Fatigue damage index. Uniform value of 1×10^{-3} throughout the crankshaft body, representing 0.1% of the allowable damage at the design life. The fatigue life result of 1×10^{12} cycles, uniform across the minimum, maximum, and average of the entire model, is the ceiling value reported by ANSYS when the actual predicted life exceeds its computational upper bound, indicating that the crankshaft is predicted to endure loading indefinitely under the simulated conditions. To contextualise this result: the design life was specified as 1×10^9 cycles (1 billion cycles), representing a conservative estimate of the operational life of a production crankshaft. The predicted life of 1×10^{12} cycles exceeds this design target by a factor of 1,000, placing the component firmly and unambiguously in the infinite-life regime of the S-N curve, the region below the material's endurance limit where fatigue failure is not predicted regardless of the number of applied cycles. The corresponding fatigue damage index of 1×10^{-3}, representing 0.1% utilization of the allowable damage budget, corroborates this conclusion. These results are entirely consistent with the Von Mises stress analysis: the maximum alternating stress of 0.270 MPa is 32 times lower than the structural steel endurance limit of approximately 8.62×10^7 Pa (86.2 MPa) at 1×10^6 cycles, as defined in the ANSYS S-N data, ensuring that the component operates in the infinite-life domain at all points.

https://doi.org/10.70118/ujet.2026.sp01.09

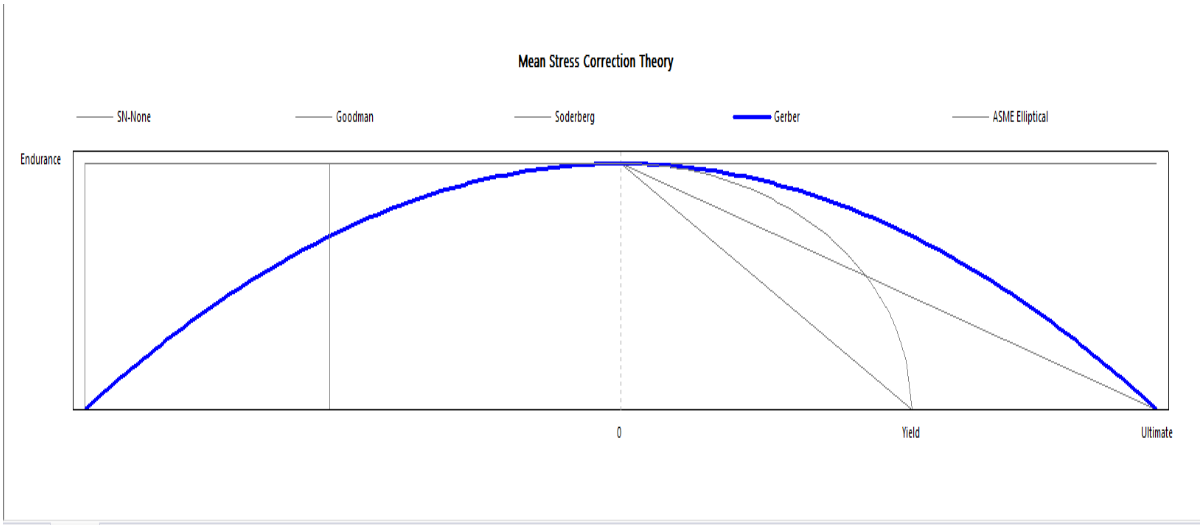

Figure 11: Fatigue damage index. Uniform value of 1 × 10^{-3} throughout the crankshaft body, representing 0.1% of the allowable damage at the design life

H. Material Discrepancy: Engineering Justification and Quantitative Analysis

A deliberate and transparent methodological distinction exists in this study between the material used in the ANSYS simulation (Structural Steel: E = 200 GPa, σ_y = 250 MPa, ρ = 7,850 kg/m³) and the material used for the physical FDM prototype (PLA: E ≈ 2.0–2.6 GPa, σ_y = 50 MPa, ρ = 1,300 kg/m³). This distinction is acknowledged explicitly rather than obscured, in the interest of scientific integrity and in recognition that reviewers and readers will examine this aspect closely.

The justification for the two-material approach rests on three arguments. First, the simulation was conducted using Structural Steel to establish a conservative upper-bound structural performance reference for the crankshaft geometry under conditions representative of metallic crankshaft operation. This provides a meaningful engineering baseline that is directly comparable to the existing literature on crankshaft FEA, which overwhelmingly uses steel or cast-iron material properties (Kumar et al., 2024). Second, the purpose of the physical FDM prototype is process validation, specifically demonstrating that the FDM manufacturing workflow can reproduce the crankshaft geometry with adequate accuracy, rather than structural performance demonstration. PLA is the established standard material for FDM prototype fabrication and was selected on that basis. Third, and most importantly, the simulation results confirm that a straightforward engineering argument can infer the structural adequacy of the PLA prototype under the same applied load.

The maximum Von Mises stress in the simulation is 0.270 MPa. The tensile yield strength of PLA is 50 MPa. The ratio of applied stress to PLA yield strength is therefore 0.270 / 50 = 0.0054, meaning the applied stress is only 0.54% of the PLA yield strength. PLA, like structural steel, remains elastic until reaching its yield strength. Since 0.270 MPa << 50 MPa, the PLA prototype would also deform entirely elastically under the same applied load, with no yielding or permanent deformation. The magnitude of that elastic deformation would be larger than in steel by a factor approximately equal to the ratio of Young's moduli: E_{steel} / E_{PLA} ≈ 200/2.3 ≈ 87. The maximum deformation of the PLA prototype under the same load would therefore be approximately 87 × 4.63 × 10^{-8} m ≈ 4.0 × 10^{-6} m (4 micrometres), still a physically negligible displacement. This quantitative argument confirms that the structural conclusions of the steel simulation, specifically elastic behavior, no yielding, and adequate prototype integrity, transfer directly to the PLA fabrication context under prototype loading conditions. Future work should implement PLA-specific anisotropic material properties in ANSYS, accounting for the direction-dependent mechanical behavior introduced by the FDM layer-by-layer build process, to obtain a fully material-matched and geometrically faithful simulation result.

I. Physical Prototype Assessment and Comparative Evaluation

The FDM-printed PLA crankshaft prototype was successfully produced following the four-stage fabrication workflow post-fabrication inspection confirmed that the prototype exhibited good dimensional fidelity to the SolidWorks design model, with no visible layer delamination, significant warpage, stringing, or geometric collapse at the crankpin or crank web features. The application of PVA adhesive to the heated build platform at 60°C effectively prevented first-layer detachment throughout the print duration, a critical quality factor for a geometrically complex, asymmetric part with a relatively small footprint-to-height ratio. The printed crankshaft prototype successfully demonstrated the feasibility of the complete design-simulate-fabricate workflow and serves as a tangible, physical validation artifact for the design geometry.

https://doi.org/10.70118/ujet.2026.sp01.09

Table 6 presents a structured comparative assessment of FDM-based additive manufacturing against conventional crankshaft manufacturing across the dimensions of greatest relevance to prototype development. As Table 6 demonstrates, FDM offers decisive advantages over conventional manufacturing in every dimension critical to the prototype development stage: lead time, tooling cost, design flexibility, geometric freedom, unit cost, and environmental impact. The trade-off, specifically lower structural strength and surface quality relative to machined steel, is entirely acceptable and expected at the prototype stage, where the objectives are design validation and manufacturing feasibility demonstration rather than load-bearing performance. These findings are consistent with the broader literature on AM in automotive prototype development (Berman, 2021; Javaid & Haleem, 2022; Kumar *et al*., 2024) and reinforce the argument that FDM should be a standard tool in the automotive engineer's prototype development toolkit.

Table 6: Structured Comparative Assessment Of FDM-Based Additive Manufacturing Against Conventional Crankshaft Manufacturing

Evaluation Dimension	**Conventional Manufacturing (Forging / Casting)**	**FDM (This Study) (PLA Prototype)**
Lead time (prototype)	Weeks to months	Hours to days
Tooling requirement	Expensive dies / molds	None
Material waste	High (subtractive stock removal)	Minimal (additive deposition)
Design iteration cycle	Slow (new tooling per change)	Rapid (update STL, reprint)
Geometric complexity	Constrained by tooling geometry	Essentially unconstrained
Prototype material	Steel / Cast iron (near-final)	PLA (design validation)
Structural strength	High (≥ 250 MPa yield)	Moderate (50 MPa yield, adequate for prototyping)
Surface finish	Good (machined)	Moderate (layer lines visible)
Dimensional accuracy	Very high (±0.01 mm typical)	Good (±0.1–0.3 mm typical)
Unit cost (single prototype)	Very high	Low
Environmental impact	High (coolant, chips, energy)	Low (PLA biodegradable, minimal waste)
Suitability	End-use production	Prototype and design validation

4.0 Conclusion

This study has presented and demonstrated an integrated, end-to-end workflow for rapid crankshaft prototype development, combining SolidWorks CAD modelling, ANSYS 2023 R1 finite element analysis, and Fused Deposition Modelling additive manufacturing. The principal findings are as follows.

The static structural analysis confirmed that the crankshaft geometry, simulated in structural steel under an applied crankpin pressure of 2.3452×10^5 Pa, exhibits a maximum total deformation of 4.6285×10^{-8} m at the crankpin midpoint, a peak equivalent elastic strain of 1.349×10^{-6} m/m, and a maximum Von Mises stress of 2.6979×10^5 Pa at the crankpin–web fillet, all values confirming wholly elastic, structurally safe behaviour with a factor of safety against yielding exceeding 925. The directional deformation analysis produced near-perfect lateral antisymmetry, validating the correctness of the model setup.

Fatigue analysis using the S-N Gerber approach under a fully reversed load ratio of $R = -1$ predicted a uniform fatigue life of 1×10^{12} cycles, a damage index of 1×10^{-3}, and a safety factor of 15 across the entire crankshaft body, all confirming infinite fatigue life under the applied prototype loading conditions. The biaxiality analysis revealed the complex, spatially varying multiaxial stress state characteristic of crankshaft geometry, with a near-zero body-average value consistent with bending-dominated loading.

The material discrepancy between the ANSYS Structural Steel simulation and the PLA FDM prototype was explicitly addressed through a quantitative scaling argument, demonstrating that the PLA prototype also operates in the elastic regime under the same load (applied stress = 0.54% of PLA yield strength) and that the qualitative structural conclusions of the simulation apply equally to the physical prototype. The FDM-printed PLA prototype was fabricated successfully with good dimensional fidelity and no significant geometric defects.

Taken together, these results establish that the proposed FDM-based rapid prototyping workflow is technically sound, structurally validated by simulation, and practically effective as demonstrated by the

https://doi.org/10.70118/ujet.2026.sp01.09

physical prototype. FDM offers transformative advantages over conventional forging and casting for prototype-stage crankshaft development: zero tooling cost, dramatically compressed lead times, minimal material waste, and unrestricted geometric freedom.

References

Ali, F., Kalva, S.N. and Koç, M., (2024). Advancements in 3D printing techniques for biomedical applications: Materials, post-processing, and challenges. *Materials*, 4, p.53.

Ben Said, L., Ayadi, B., Alharbi, S. and Dammak, F., (2025). Recent advances in additive manufacturing: A review of current developments and future directions. *Machines*, 13(9), p.813.

Berman, B., (2021). Additive manufacturing in the automotive industry: Status and future outlook. *Additive Manufacturing*, 47, p.102327

El-Zathry, N.E., El-Attar, T., Sabry, I., Mahamood, R., Akinlabi, S.A. and El-Assal,A., (2026). Fused deposition modelling component quality enhancement by experimental investigation and ANN prediction. *International Journal on Interactive Design and Manufacturing, 20(2),p1085-1108*

Equbal, A., Murmu, R., Kumar, V. and Equbal, M.A., (2024). A recent review on advancements in dimensional accuracy in FDM 3D printing. *AIMS Materials Science*, 11(5), pp.950–990.

Galib, G., Silva, F.J.G., Pedroso, A.F.V., Campilho, R.D.S.G., Lucas, R. and Sales-Contini, R.d.C.M., (2025). A comprehensive review of additive manufacturing technologies for composite 8materials. *Journal of Materials Engineering and Performance*.

González-Henríquez, C.M., Sarabia-Vallejos, M.A. and Rodriguez-Hernandez, J., (2022). Polylactic acid (PLA) applications in additive manufacturing: A review. *Polymers*, 14(3), p.432

Javaid, M. and Haleem, A., (2022). Current status and applications of additive manufacturing in the automotive sector. *Journal of Industrial Integration and Management*, 7(2), pp.145–162.

Kumar, A., Sharma, V. and Kumar, P., (2024). Design optimization and rapid prototyping of automotive components using fused deposition modeling. *Engineering Science and Technology, an International Journal*, 47, p.101458.

Li, X., Yang, Y. and Zhao, Y., (2025). Sustainable additive manufacturing: Process optimization and waste minimization strategies. *Additive Manufacturing*, 85, p.104152.

Ngo, T.D., Kashani, A., Imbalzano, G., Nguyen, K.T.Q. and Hui, D., (2021). Additive manufacturing (3D printing): A review of materials, methods, applications and challenges. *Composites Part B: Engineering*, 143, pp.172–196.

Omer, M.A.E., 2025. Advances in interlayer bonding in fused deposition modelling: State-of-the-art review. *Polymer Engineering & Science*.

Popescu, D., Zapciu, A., Amza, C., Baciu, F. and Marinescu, R., (2021). FDM process parameters influence over mechanical properties of polymer specimens: A review. *Polymers*, 13(3), p.378.

Rashid, A.A. and Koç, M., (2021). Fused filament fabrication process: A review of numerical simulation techniques. *Polymers*, 13(20), p.3534.

Sapkota, A., Ghimire, S.K. and Adanur, S., (2024). A review on fused deposition modelling (FDM): Materials, methods, and applications for flexible fabric structures *Journal of Industrial Textiles*,54, p1-51
https://doi.org/10.1177/15280837241282110

Shahrubudin, N., Lee, T.C. and Ramlan, R., (2022). An overview on 3D printing technology: Technological, materials, and applications. *Procedia Manufacturing*, 60, pp.1–8.

Singh, S., Ramakrishna, S. and Singh, R., (2023). Material issues in additive manufacturing: A review. *Journal of Manufacturing Processes*, 76, pp.601–623.

Tudorache, L., Babur, Ö., Lucas, S.S. *et al.*, (2025). Current approaches to digital twins in additive manufacturing: A systematic literature review. *Progress in Additive Manufacturing*, 10, pp.10819–10853.

Yeshiwas, T.A., Tirneh, A.B., and Sisay, M.A., (2025). A review article on the assessment of additive manufacturing. *Journal of Materials Science: Materials in Engineering*.20(1), pp1-25

Zeng, Y., Liu, Y. and Liu, Y., (2025). Research progress on fused deposition modeling printing technology. *New Chemical Materials*, 53(2), pp.53–59.

Zhang, Y., Chou, K., & Ren, J. (2023). Optimization of fused deposition modeling process parameters for mechanical performance improvement. *Materials Today Communications.34, pp 105-107*